

Effect of high temperature exposure on epoxy-coated glass textile reinforced mortar (GTRM) composites

Original

Effect of high temperature exposure on epoxy-coated glass textile reinforced mortar (GTRM) composites / Messori, M.; Nobili, A.; Signorini, C.; Sola, A.. - In: CONSTRUCTION AND BUILDING MATERIALS. - ISSN 0950-0618. - 212:(2019), pp. 765-774. [10.1016/j.conbuildmat.2019.04.026]

Availability:

This version is available at: 11583/2878995 since: 2021-03-31T12:23:47Z

Publisher:

Butterworth Heinemann Publishers

Published

DOI:10.1016/j.conbuildmat.2019.04.026

Terms of use:

This article is made available under terms and conditions as specified in the corresponding bibliographic description in the repository

Publisher copyright

(Article begins on next page)

Effect of high temperature exposure on epoxy-coated glass textile reinforced mortar (GTRM) composites

Massimo Messori^a, Andrea Nobili^a, Cesare Signorini^{b,c,*}, Antonella Sola^a

^a*Dipartimento di Ingegneria Enzo Ferrari, via Vivarelli 10, 41125 Modena, Italy*

^b*Dipartimento di Scienze e Metodi dell'Ingegneria, via Amendola 2, 42122 Reggio Emilia, Italy*

^c*Dipartimento di Economia, Scienze e Diritto, Via Consiglio dei Sessanta 99, 47899 Dogana, Republic of San Marino*

Abstract

An experimental investigation on the mechanical performance of epoxy-coated Alkali-Resistant (AR) glass textile reinforced mortar subjected to elevated temperature is presented. Two epoxy coatings are considered, which differ by the hardening agent alone. After 56 days dry curing, specimens are heated up to four different temperatures. After cooling down to ambient temperature, specimens are assessed in uni-axial tensile test according to Annex A of AC434. First cracking strength and elongation, ultimate tensile strength and elongation, cracked and uncracked moduli, transition point location and energy dissipation capability are evaluated. It is found that, in the explored temperature range, degradation is surprisingly mild and strongly dependent on the resin which is taken as coating agent. Indeed, temperature exposure may lead to strength enhancement. This positive outcome takes place at the expense of ductility and it is traced back, through Differential Scanning Calorimetry (DSC), to a post-curing process. Nonetheless, energy dissipation still decreases with temperature and, remarkably, with the same power-law behaviour for both resins. Such behaviour is compatible with a cumulative Weibull distribution, that is adopted in thermal damage models for resins, and it indicates that the underlying damage mechanism indeed operates on the resin at the fabric-to-matrix interface.

*Corresponding author

Email address: cesare.signorini@unimore.it (Cesare Signorini)

Keywords: TRM, High temperature, Epoxy coating

1. Introduction

1 The possibility of high temperature exposure poses a serious limitation to
2 the applicability of organic matrix reinforcing systems, such as fibre-reinforced
3 polymers (FRPs). Indeed, exposing FRP systems to temperatures in excess of
4 or even close to the glass transition temperature T_g produces a substantial and
5 sudden drop in the mechanical response [10, 6]. This behaviour, that rapidly
6 leads to delamination and failure, is all the more undesired in consideration of
7 the fairly low transition temperature $T_g \approx 80^\circ\text{C}$ characterizing most organic
8 resins. In this respect, Textile Reinforced Mortar/Cement (TRM/TRC) and
9 Fabric Reinforced Cementitious Matrix (FRCM) composite materials exhibit
10 vastly superior thermal stability, in light of the adoption of an inorganic matrix.
11 On the other hand, the bond strength between the fabric and the inorganic
12 matrix is generally weak and this leads to poor mechanical performance and
13 a generally inconsistent failure pattern [2, 21]. Improvement in the matrix-to-
14 fabric bond may be obtained by adopting inorganic [13, 31] or organic [29, 9, 19]
15 coatings. Consequently, investigation of the effect of temperature exposure on
16 TRM is complicated by the need to consider the whole composite package, which
17 consists of the matrix, the fabric and the coating.

18 A large body of literature is devoted to the characterization of FRP systems
19 subjected to elevated temperature, see, for instance, [10, 7, 4, 28, 16, 15] and
20 references therein. Conversely, a limited number of studies is available concern-
21 ing the effect of high temperature exposure on TRM and FRCM and these are
22 mainly focused on carbon and PBO fabrics [24, 34]. In this framework, a crucial
23 issue that requires careful investigation is the role played by high temperature
24 exposure on the adhesive behaviour of the laminates at the mortar-to-substrate
25 interphase, as discussed by Ombres [23] and Maroudas and Papanicolaou [18]
26 for concrete and masonry structures, respectively. The former study presents
27 single-lap shear tests on PBO-FRCM laminates applied on concrete supports

28 and reports that conditioning at 50 °C and 100 °C affects not only the load-
29 bearing capacity of the composite, which decreases from 25 to 40% depending on
30 the number of layers, but also the failure and the delamination modes. Indeed,
31 failure statistically changes from matrix-to-fabric slippage for the unconditioned
32 samples to debonding at matrix-to-concrete interphase for the conditioned ones.
33 Analogously, in the contribution by Maroudas and Papanicolaou [18], single-lap
34 shear tests are conducted on G-TRM thin laminates applied to brick panels
35 and exposed to temperatures up to 300 °C. It is shown that, if the tempera-
36 ture exceeds 100 °C, failure is mainly triggered by adhesive debonding at the
37 masonry-to-mortar interphase and strongly affected by the deterioration of the
38 ultimate strength of the bare glass fabric. Furthermore, Raouf and Bournas [26]
39 and Bisby et al. [3] assess the response in bending of TRM and FRP reinforcing
40 systems subjected to high temperatures, while Tetta and Bournas [32] considers
41 jacketing. Trapko [33] compares FRP and FRCM confined concrete elements
42 exposed to temperatures up to 80 °C for 24 h. Already at 40 °C compressive
43 strength of FRP jacketed elements is reduced by 20% and at 80 °C ductility
44 drops by 50%, as opposed to a 11% loss encountered for FRCM. de Andrade
45 et al. [8] investigate double-sided pull-out strength of an epoxy coated carbon
46 yarn after 120 min exposure at 100 °C, 150 °C, 200 °C, 400 °C and 600 °C. Max-
47 imum pull-out force and pull-out work are computed and compared with the
48 dry yarn. Interestingly, an increase in mechanical performance of the coated
49 specimens is observed after heating at temperatures up to 150 °C, that is as-
50 cribed to a "polymer interlocking mechanism in the yarn-matrix interface, which
51 is generated during the heating and cooling of the polymer yarn coating". In
52 Rambo et al. [25], uni-axial tensile tests of basalt textile reinforced plates are
53 conducted. The basalt fabric is coated with styrene-acrylic latex and refractory
54 concrete is adopted as matrix. Plates are exposed for 60 min at temperatures
55 in the range 75–1000 °C. It is found that performance loss is mild up to 200 °C
56 and it is concluded that "the presence and the type of coating can become a de-
57 terministic factor in the tensile response of the composite submitted to elevated
58 temperatures". Recently, Donnini et al. [9] present experimental and numeri-

59 cal results on the mechanical performance of dry and epoxy-plus-sand coated
60 carbon FRCM composites under uni-axial tension and double-shear bond test.
61 Beside ambient temperature, 120 min exposure at 80 °C and at 120 °C are con-
62 sidered. **It is worth emphasizing that mechanical tests are carried out inside**
63 **the climatic chamber, where specimens are exposed at high temperature.** An
64 impressive 70% drop in the ultimate tensile strength (and a 54% elongation loss)
65 is determined with respect to the ambient condition already at 80 °C.

66 In general, the existing literature lacks from detailing the thermo-physical
67 properties of the coating agent, that is usually adopted taking an out-of-the-
68 box approach. In this work, we focus on the role of epoxy coating on the
69 thermal deterioration of the matrix-to-fabric interface. To this aim, the same
70 pair of epoxy resins considered in [19] are adopted, which differ only by the
71 hardening agent. This feature, however, leads to important differences in terms
72 of thermo-physical properties that exert a profound influence on the behaviour
73 upon high temperature exposure [12]. To avoid degradation of the lime mortar
74 and restrict attention to the epoxy coating, temperature exposure is limited in
75 the range 20–250 °C and 56-day dry curing is adopted. Mechanical performance
76 is assessed in uni-axial traction of rectangular coupons according to Annex A
77 of the guidelines [14]. DSC analysis supports the conclusion that, depending
78 on the resin formulation, high temperature exposure may benefit strength (at
79 the expense of ductility), inasmuch as it promotes cross-linking in a post-curing
80 process. This mechanism is likely to explain the outcome of the double pull-out
81 tests carried out in [8] and of the uni-axial traction of plates described in [25].

82 **2. Materials and methods**

83 *2.1. Materials*

84 *2.1.1. Reinforcing fabric and inorganic matrix*

85 The commercially available Alkali Resistant Glass (ARG) fabric Zirconglass
86 Wire[©] RV320-AR (Fibre Net Spa) is adopted as fabric reinforcement. This is
87 a balanced bi-axial open-squared mesh whose 19% weight content of Zirconium
88 Oxide (ZrO₂) imparts resistance to the alkaline mortar environment. The main

Table 1: ARG Fabric mechanical properties (tex = g/km)

Characteristic	Unit	Value
Yarn count	tex	1200
Net specific weight per unit fabric area	g/mm ²	300
Fabric specific weight	g/cm ³	2.50
Grid spacing (square grid)	mm	12
Equivalent thickness, t_f	mm	0.06
Ultimate strength along warp (with epoxy)	MPa	1200
Ultimate elongation along warp	mstrain	20
Elastic modulus	GPa	74

Table 2: Mortar properties

Characteristic	Unit	Value
Nominal setting water content	%	21.2
Final density	g/cm ³	1.58
Min. compression strength after 28 days	MPa	15.0
Min. flexural strength after 28 days (EN 196/1)	MPa	5.0
Min. support adhesion strength after 28 days	MPa	1.0
Aggregate maximum size	mm	1.4
Compression elastic modulus (EN 13412)	GPa	9.0

89 properties of the fabric, **as given by the manufacturer**, are collected in Table 1.
 90 A pre-mixed natural hydraulic lime (NHL) mortar GeoCalce Fino[®] (Kerakoll
 91 SpA), aimed at structural purposes, constitutes the inorganic embedding matrix.
 92 Table 2 gathers the main properties of this fine-grained repair mortar **as given**
 93 **by the manufacturer**.

94 *2.1.2. Fabric sizing and coating*

95 ARG fabric is subjected, as received, to a preliminary sizing treatment to en-
 96 hance chemical compatibility with the epoxy coating. Following the procedure

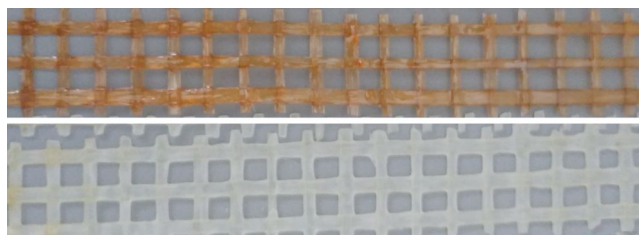


Figure 1: Coated fabric before the heat treatment (upper: ER, lower: EW)

Table 3: Hardening agents datasheet

Characteristic	Unit	m-PDA	DETA
Physical form	-	Pellets	Liquid
Formula	-	$C_6H_8N_2$	$C_4H_{13}N_3$
Melting point	$^{\circ}C$	63÷65	-40
Flash point	$^{\circ}C$	175	94
Boiling point	$^{\circ}C$	282÷284	200÷204

97 described in [19], fabric is functionalized by immersion in a 2% vol. aqueous
 98 solution of (3-Aminopropyl)triethoxysilane (99%, Sigma-Aldrich), which takes
 99 on the role of coupling agent. Care is taken to avoid organic solvents which may
 100 damage the thermoplastic stitches that hold the unwoven fabric. Fabric is then
 101 dried in ambient air. Fabric epoxy coating is obtained from high-purity bisphe-
 102 nol A diglycidylether resin D.E.R. 332, (DOW Chemicals, hereafter "DER").
 103 Two coatings are considered, named ER and EW, which only differ by the curing
 104 agent: ER exploits the aromatic hardener m-phenylenediamine (99%, Acros Or-
 105 ganics hereafter "m-PDA"), while EW adopts the aliphatic diethylenetriamine
 106 (99%, Alfa-Aesar hereafter "DETA"). Table 3 presents the main characteristics
 107 of the curing agents **as declared by the producers**, with particular emphasis on
 108 thermal properties. The coated fabric is laid on a polypropylene sheet to pre-
 109 vent warping, which may hinder the lamination process, and then it is allowed
 110 to set for 7 days at laboratory conditions (Fig.1).

111 2.1.3. Specimen manufacturing

112 1-ply ARG-TRM coupons are manufactured on an individual basis by means
 113 of a dismountable polyethylene formwork, following a well-established and reli-
 114 able manufacturing protocol, see [30, 22]. The lubricated surface of the formwork
 115 is segmented by 3mm-thick laths, equally spaced according to the specimen
 116 width. In between adjacent laths, uniformly-thick mortar layers are laid out.
 117 Indeed, the top surface of the laths provides an easy reference for scraping off
 118 the mortar in excess of 3 mm. Cut-to-size glass fabric is laid on top of the fresh
 119 mortar and gently pressed on it. Then, a second array of polyethylene laths is
 120 pinned on top of the first to provide reliable fabric placing as well as reference



Figure 2: Manufacturing process of the specimens: application of the second set of constraining laths for uniform placement of the second layer of mortar

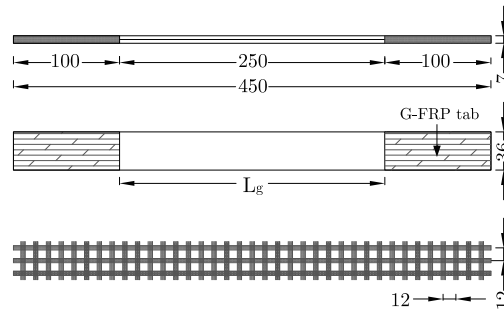


Figure 3: Coupon and fabric mesh geometries

121 for laying out the second mortar layer (Figure 2). At the final stage of their
 122 placing, laths are covered with paper adhesive tape to ease specimen stripping.
 123 A minimum of four specimens is considered for each test group. 7-day moist
 124 curing is followed by dry curing at room temperature for 56 days in total. In-
 125 deed, curing time is proven to deeply affect the mechanical performance of lime
 126 and cement-based composites [22] and their resistance to aggressive environ-
 127 ments [20]. The specimen geometry (coupon) is schematically drawn in Fig.3
 128 alongside the fabric mesh size. **After heating and natural cooling**, a pair of ex-
 129 ternally bonded 100-mm G-FRP tabs is glued at both ends of each specimen to
 130 accommodate the clamps of the testing machine.

Table 4: High temperature exposure conditions in the literature

Ref.	Temp. [°C]	Exp. time [min]	Composite	Test
Xu et al. [34]	120, 200	30, 90	CFRCM+epoxy	3-point bending
Donnini et al. [9]	20, 80, 120	100	CFRCM+epoxy	uni-axial traction, double shear bond
de Andrade et al. [8]	100, 150, 200, 400, 600	120	CFRCM+epoxy	double sided pull-out
Trapko [33]	40, 60, 80	1440	CFRCM	compression of confined cylinders
Rambo et al. [25]	75, 150, 200, 300, 400, 600, 1000	60	basalt+latex+FRCM	traction of plates
Ombres [23]	20, 50, 100	480	PBO-FRCM	single-lap shear
Ombres [24]	20, 50, 100, 150, 200, 250	1200	PBO-FRCM	compression on confined cylinders
Maroudas and Papanicolaou [18]	20, 100, 200, 300	1200	GFRCM	single-lap shear

131 2.2. High temperature exposure

132 After curing, coupons undergo a heating treatment in a Binder WTC oven.
133 A 4 °C/min heating ramp is applied until either of four different target tempera-
134 tures is reached, namely 100, 150, 200 or 250 °C. The set of target temperatures
135 is chosen to induce coating degradation only. Indeed, according to [5], fabric
136 composites in a cement-based matrix perform well up to 450 °C. Once the target
137 temperature is attained, isothermal conditions are maintained for 120 min. It
138 should be observed that heating time and target temperature are not standard
139 and indeed they vary greatly across the relevant literature, as summarized in
140 Tab.4. Specimens are then moved to room temperature ($20 \pm 2^\circ\text{C}$) and left to
141 cool down in a natural cooling process, as in [8].

142 3. Experimental characterization

143 3.1. Optical investigation

144 Preliminary visual investigation of the specimens after heating is illustrated
145 in Fig.4. In particular, both epoxy coatings, when exposed to temperatures

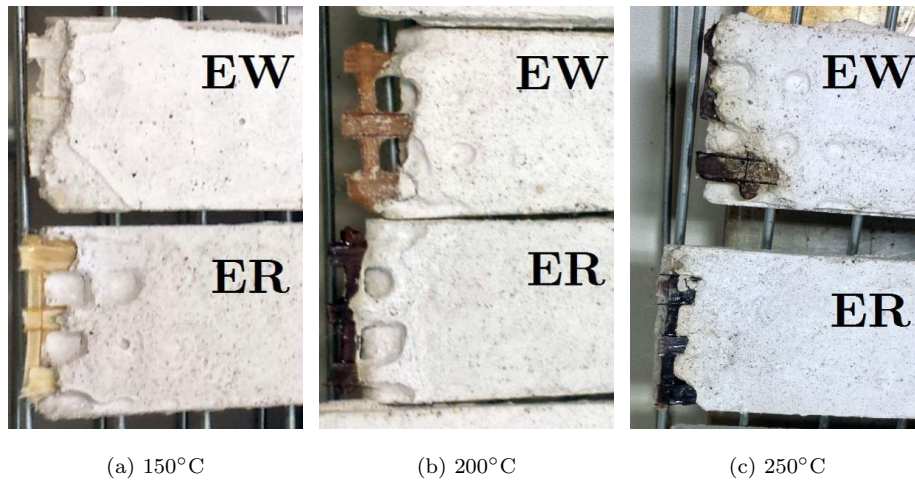


Figure 4: Mortar and fabric after temperature exposure: it clearly appears that both epoxy coatings oxidise above 150 °C

146 higher than 150 °C, appear oxidized and blackened (compare with the uncoated
 147 fabric shown in Fig.1), while little to no effect is visible at lower temperature.
 148 Mortar appears unaffected by any temperature.

149 3.2. Differential Scanning Calorimetry

150 A Differential Scanning Calorimetry (DSC) analysis (TA DSC 2010, TA
 151 Instruments, New Castle, DE, USA) is performed on both epoxy resins, EW and
 152 ER, in a single heating ramp, starting from 0 °C up to 250 °C, with a heating rate
 153 of 10 °C/min, under nitrogen flow. The analysis is conducted at two different
 154 stages, namely immediately after resin preparation ("as mixed" condition) and
 155 after two-week curing at ambient temperature. Comparing the heating enthalpy
 156 developed in the two conditions yields the *conversion degree*, that measures the
 157 extent to which cross-linking may occur at ambient temperature.

158 3.3. Uni-axial monotonic tensile test

159 Following the guidelines [14], mechanical performance is assessed in uni-
 160 axial tensile test. A Instron 5567 electromechanical Universal Testing Machine
 161 (UTM) is employed. The UTM is equipped with a 30 kN load cell and a pair
 162 of wedge clamps which, as specified in [14, §A2.2], "shall apply sufficient lateral

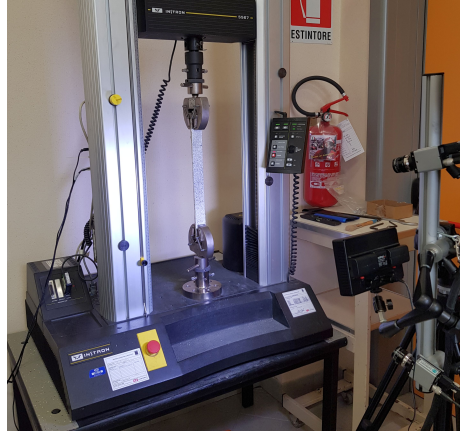


Figure 5: Uni-axial tensile test set-up with DIC monitoring of the speckled specimen

163 pressure to prevent slippage between the grip face and the coupon”. Besides,
164 rotationally self-aligning grips are adopted, ”to minimize bending stresses in
165 the coupon”. Tests are performed under displacement control at a nominal dis-
166 placement rate of 0.5 mm/min, that complies with the elongation rate proposed
167 by the RILEM committee [27].

168 As already pointed out in [20], for the correct determination of elastic moduli,
169 transition points and of the strain evolution during testing, the sliding displace-
170 ment occurring in the wedge clamps needs to be subtracted from the nominal
171 elongation ramp. To this aim, a Dantec Dynamics Q400 Digital Image Corre-
172 lation (DIC) system is employed to measure the actual specimen displacement.
173 Indeed, comparison of the nominal data with the DIC-measured elongation re-
174 veals a $8 \div 10\%$ discrepancy in strain evaluation. The test set-up is shown in
175 Fig.5.

176 4. Results

177 4.1. Mechanical performance

178 Fig.6 presents the mean strength curve for all test groups. As customary,
179 strength is reported to the coated fabric cross-section and strain is normalized
180 against the gauge length L_g . It immediately appears that the EW group perfor-
181 mance is significantly impaired by the heating conditioning at any temperature,

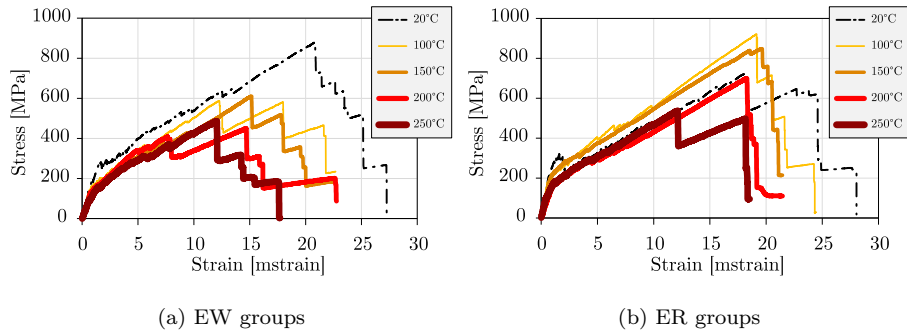


Figure 6: Mean stress-strain curve for the control (black, dashed-dotted line) and the exposed groups (solid lines with increasing thickness in dependence of the temperature exposure), namely 100 °C (yellow), 150 °C (orange), 200 °C (red) and 250 °C (amaranth)

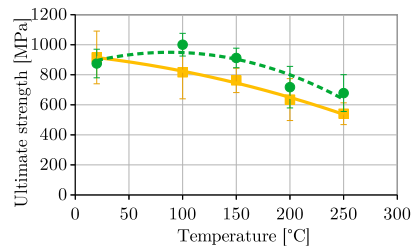


Figure 7: Mean ultimate tensile strength as a function of the exposure temperature for ER (circles, green) and EW (squares, yellow). ± 1 standard deviation bars and parabolic curve-fits are also presented

Table 5: Mean first cracking strength (FCS), ultimate tensile strength (UTS), uncracked and cracked moduli for the EW group as a function of the exposure temperature. CV is the coefficient of variation

T [°C]	FCS		UTS		E_f^*		E_f	
	$\mu(f_{cr})$ [MPa]	CV [%]	$\mu(f_u)$ [MPa]	CV [%]	$\mu(E_f^*)$ [GPa]	CV [%]	$\mu(E_f)$ [GPa]	CV [%]
20	271.0	23.1	915.6	19.2	249.7	20.5	30.8	23.1
100	163.1	14.0	816.3	21.6	190.9	12.6	37.4	14.0
150	154.2	15.0	762.7	10.7	193.8	38.1	34.7	1.5
200	165.1	42.0	634.8	22.0	162.8	21.7	39.0	42.0
250	168.8	51.2	540.7	13.4	160.8	41.0	29.8	51.8

Table 6: Mean first cracking strength (FCS), ultimate tensile strength (UTS), uncracked and cracked moduli for the ER group as a function of the exposure temperature. CV is the coefficient of variation

T [°C]	FCS		UTS		E_f^*		E_f	
	$\mu(f_{cr})$ [MPa]	CV [%]	$\mu(f_u)$ [MPa]	CV [%]	$\mu(E_f^*)$ [GPa]	CV [%]	$\mu(E_f)$ [GPa]	CV [%]
20	192.4	24.4	875.0	10.9	319.7	21.1	31.0	15.0
100	183.3	16.4	1000.3	7.6	286.1	18.6	40.1	7.2
150	225.5	5.9	912.0	7.1	250.9	10.1	35.3	10.2
200	135.4	30.3	717.6	19.3	156.4	1.8	32.4	22.2
250	124.5	29.5	678.0	18.1	187.4	18.7	37.2	6.8

182 while the ER groups exhibit a mixed response. Results in terms of first crack-
183 ing strength, ultimate tensile strength (UTS), cracked and uncracked moduli
184 are summarized in Tab.5 for EW and in Tab.6 for ER. This behaviour is bet-
185 ter illustrated by the curves of Fig.7, which compare the mean ultimate tensile
186 strength (UTS) across the two groups. Indeed, while the mean UTS across the
187 EW group decreases monotonically with the exposure temperature, it increases
188 significantly in the ER-100 group and marginally in the ER-150 group, before
189 it starts to decay. Data scattering for elastic moduli is presented in Fig.8 as
190 a function of the conditioning temperature. Parabolic curve-fitting shows that
191 scattering decreases upon temperature exposure up to a critical temperature
192 that is connected to a post-curing phenomenon, as discussed in Sect.4.2.

193 In general, even for EW, heat conditioning has a surprisingly limited effect on
194 the performance decay of the coated fabric, especially when results are compared

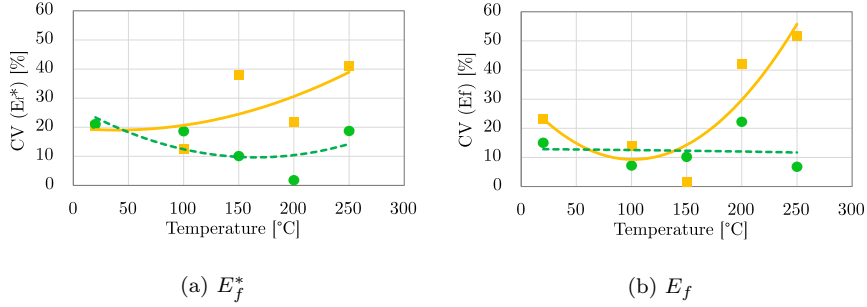


Figure 8: Coefficient of Variance (CV) for the uncracked (a) and cracked (b) secant moduli as a function of the exposure temperature for EW (orange) and ER (green) alongside its parabolic curve-fit. It is seen that post-curing positively affects data scattering as well as absolute performance

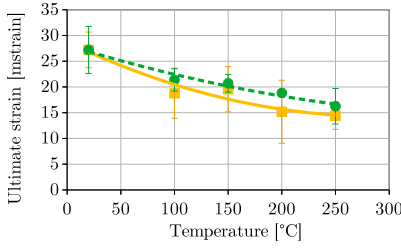


Figure 9: Mean ultimate strain values as a function of the exposure temperature for ER (circles, green) and EW (squares, yellow). ± 1 standard deviation bars and parabolic curve-fits are also presented

195 with the existing literature. In fact, although the performance pattern of ER is
 196 similar to that observed in [8, Fig.5] in the context of a double-sided pull-out
 197 test of a epoxy coated carbon multi-filament yarn, it should be remarked that,
 198 in the absence of a DSC analysis, the polymer coating adopted there seems
 199 exceptionally thermostable, for it cross-links at 160 °C and “the polymer film
 200 remained stable at temperatures up to 200 °C”.

201 Fig.9 presents a similar comparison of the mean ultimate strain at failure
 202 and it shows that ductility decreases with temperature through a similar trend
 203 for both coatings.

204 4.2. Thermal analysis

205 The DSC analysis reveals an exothermic peak for both resins, associated
 206 to two-week post-curing in ambient conditions. In order to estimate the con-

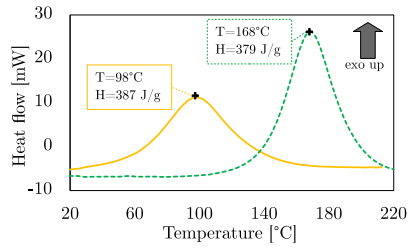
Table 7: Specific enthalpy associated to curing (H_{curing}) of as-mixed and two-week-cured EW and ER resins and corresponding conversion degree.

Resin	H_{curing} [J/g]		Conversion degree [%]
	as mixed	two-week cured	
EW	387	15	96
ER	379	123	67

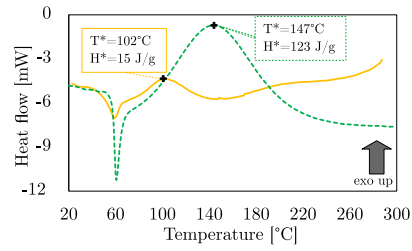
207 version degree that could be achieved, the specific enthalpy measured from the
 208 DSC thermograms of Fig.10 in the two-week-cured group is compared to the
 209 corresponding value obtained in the "as-mixed" group, as summarized in Table
 210 7. For EW, the specific enthalpy associated to curing is located at 387 J/g in the
 211 as-mixed condition and plunges to 15 J/g (corresponding to less than 4%) after
 212 two-week curing at ambient temperature. Consequently, two-week curing lends
 213 a conversion degree of about 96% when DETA is employed as curing agent.
 214 The same procedure applied to ER (that is when m-PDA acts as curing agent)
 215 reveals that the conversion degree achieved after two week curing at ambient
 216 temperature is much lower: about 67%. In fact, aliphatic amines allow curing at
 217 room temperature, whereas aromatic amines usually require a high-temperature
 218 treatment to achieve full conversion. However, aromatic amine-cured systems
 219 can be applied at temperatures sensibly higher than those which are compatible
 220 with aliphatic amine-cured resins [12, p.168]. The completion of the curing pro-
 221 cess and the high thermal stability that is typical of amine-cured epoxy resins
 222 are likely responsible for the increase in mechanical properties (elastic modulus
 223 and strength) that is observed in the epoxy-coated G-TRM composite materials
 224 that were treated at temperatures not exceeding 150 °C. At higher temper-
 225 ature, degradative phenomena are likely to outweigh the benefit conveyed by
 226 post-curing.

227 4.3. Failure analysis

228 Fig.11 illustrates progression to the two typical failure modes: either fabric
 229 rapture (a) or fabric slippage inside the matrix (b). Although, generally, both
 230 of them occur in mixed proportion in all test groups, fabric failure is far more

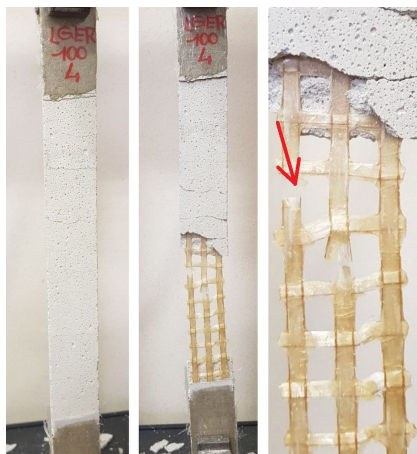


(a) Resins "as mixed"

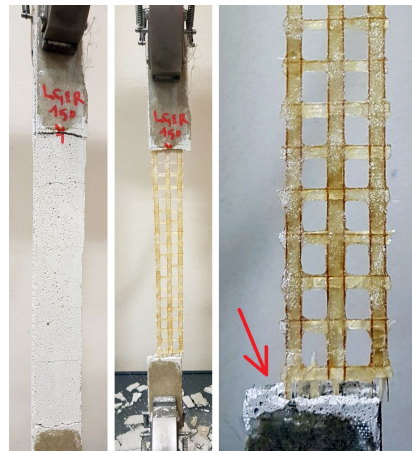


(b) Two-week cured resins

Figure 10: Differential scanning calorimetry (DSC) of EW resin (solid, yellow) and ER resin (dashed, green) right after mixing (a) and after two-week curing (b)



(a) Fabric failure



(b) Fabric slippage within the matrix and near the clamps

Figure 11: Typical failure modes observed for all groups

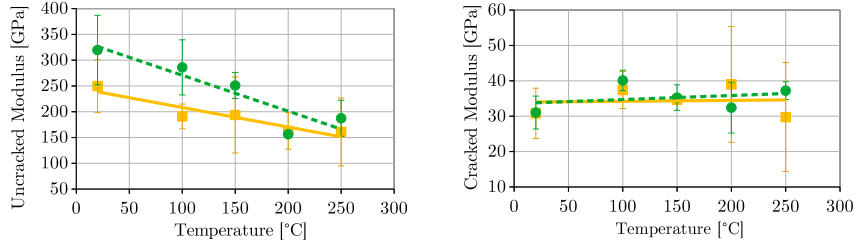


Figure 12: Uncracked (left) and cracked (right) modulus as a function of the exposure temperature for ER (circles, green) and EW (squares, yellow). ± 1 standard deviation bands and linear curve-fits are also given

231 frequent in the control group, while fabric slippage prevails in the specimens
 232 exposed to high temperature.

233 5. Discussion

234 Fig.12 illustrates the effect of temperature on the uncracked modulus E_f^*
 235 and on the cracked modulus E_f in the EW and in the ER group (see [14, 1]
 236 for the details of moduli definition and evaluation). It may be observed that
 237 temperature exposure strongly impairs the uncracked modulus E_f^* , while the
 238 cracked modulus E_f remains statistically unaltered. **This is compatible with**
 239 **the expectation that temperature affects the coating performance, whose bear-**
 240 **ing is mostly relevant when the matrix is still collaborating with the fabric and**
 241 **thereby uncracked. Furthermore, although ER coating performs significantly**
 242 **better than EW, line fitting suggests that this advantage decreases with tem-**
 243 **perature until equal performance is met at $T = 250^\circ\text{C}$. Conversely, the cracked**
 244 **modulus E_f reflects the modulus of the glass fabric, which is little affected by**
 245 **temperature. In fact, the cracked modulus is about the same across all groups.**

246 Transition points (TPs) conventionally mark a sudden stiffness loss and a
 247 regime shift, in light of the fact that the cracked matrix ceases to contribute
 248 to the composite rigidity. Their location is shown in Fig.13 at different tem-
 249 peratures. This figure indicates that the transition stress nearly halves on high
 250 temperature exposure, irrespectively of the temperature value, in the EW group.
 251 Conversely, the ER group presents a similar transition point location for ER-100

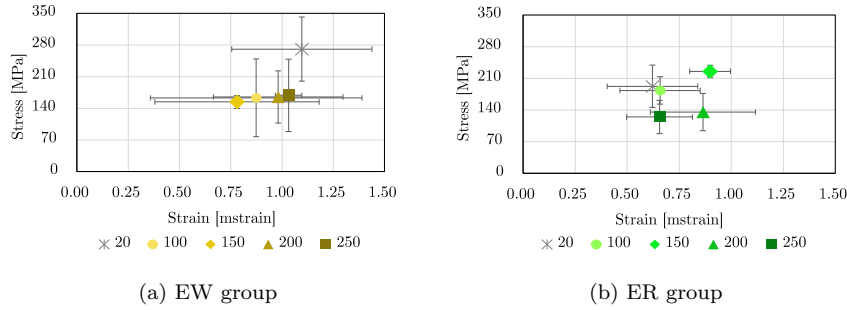


Figure 13: Mean transition point location and ± 1 standard deviation bars as a function of temperature for all test groups

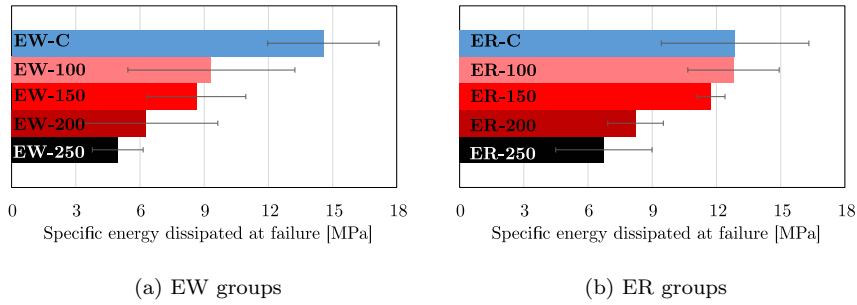


Figure 14: Mean specific energy dissipated at failure W and ± 1 standard deviation bars for the control (C, blue) and the heat treated groups at 100 °C (light red), 150 °C (red), 200 °C (dark red) and 250 °C (black).

252 and, remarkably, higher transition stress and strain for ER-150, with respect to
 253 the control group. Temperature adverse influence starts to manifest itself at
 254 200 °C, when stress is impaired (-37.5%) and yet strain is still higher than in
 255 the control group. Finally, at 250 °C, strain drops and it reaches the value for the
 256 control group. It is concluded that temperature generally decreases transition
 257 stress but it may improve transition strain.

258 Comparison in terms of specific (per unit fabric volume) dissipated energy
 259 W is carried out in Fig.14. It appears that high temperature impairs energy
 260 dissipation in all test groups, with the possible exception of ER-100 which be-
 261 behaves similarly to the relevant control group. Remarkably, both coatings decay
 262 with an almost identical power-law rule, as illustrated in Fig.15 in terms of
 263 normalized quantities with respect to the ambient conditions. This finding is

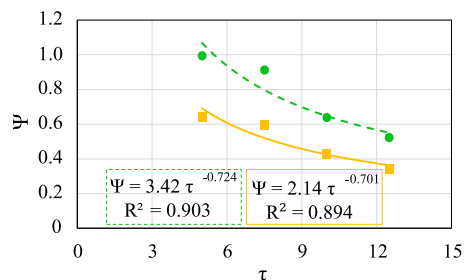


Figure 15: Normalized specific energy dissipated at failure $\Psi = W/W_0$ against normalized exposure temperature $\tau = T/T_0$ for ER (circles, green) and EW (squares, yellow) and power-law curve fit. $T_0 = 20^\circ\text{C}$ is the ambient temperature and $W_0 = W(T_0)$ is the corresponding dissipated energy.

264 compatible with a cumulative Weibull distribution for the relaxing and breaking
 265 of the intermolecular bonds in the resin, as described in the model proposed by
 266 Mahieux et al. [17], and it suggests that mechanical performance is indeed im-
 267 paired by the mechanism of resin degradation. Conversely, hyperbolic tangent
 268 models, as in [11, Eq.(5)], do not seem to fit well experimental data.

269 Fig.16 presents the behaviour of the relative ductility across all test groups
 270 against temperature at different fraction of the UTS. Relative ductility is ex-
 271 pressed as the ratio of the mean group strain $\epsilon_i(f)$, $i \in \{\text{ER}, \text{EW}\}$ over the mean
 272 control group strain $\epsilon_C(f)$, when specimens are subjected to a traction force f
 273 which is a fraction of f_{u_i} , $i \in \{\text{ER}, \text{EW}\}$, that is the UTS for the relevant group.
 274 It is clearly seen that the higher the temperature of conditioning, the more brittle
 275 specimens behave, with the single exception of 20% loading, see Fig.16(a).
 276 However, for any temperature and loading fraction, ER outperforms EW in a
 277 statistically significant manner. It is worth emphasizing that the EW group is
 278 connected to superior energy dissipation capability in the control group, as com-
 279 pared to the ER group. This advantage at ambient temperature can be traced
 280 back to the EW coating layer being significantly thinner [19]. Therefore, it may
 281 be argued that coating thickness is unfavourable in terms of ambient temper-
 282 ature mechanical performance, yet it is advantageous when high temperature
 283 exposure is envisaged.

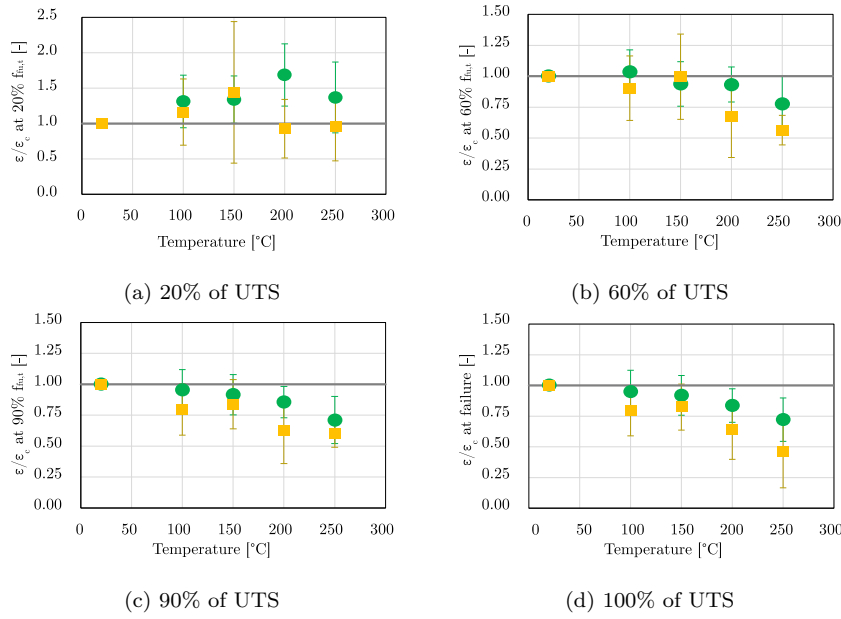


Figure 16: Ratio of the group mean elongation ϵ to the relevant control group elongation ϵ_c at a fraction of the corresponding UTS as a function of temperature for ER (circles, green) and EW (squares, yellow)

284 6. Conclusions

285 This work reports on the influence of the epoxy coating thermo-physical
 286 properties on the mechanical performance of AR-glass textile reinforced mortar
 287 (TRM) after exposure to high temperature. As in [19], two epoxy coatings
 288 are considered, which differ by the hardening agent alone. Nonetheless, this
 289 difference brings about distinct thermo-physical properties. Since focus is set
 290 on the epoxy coating, exposure temperatures are limited to 250 °C to prevent
 291 thermal effects from extending to the lime mortar and, eventually, to the glass
 292 fabric. Mechanical performance is assessed according to AC434 through uni-
 293 axial tensile tests of rectangular coupons. The effect of temperature exposure
 294 in terms of first cracking strength and strain, ultimate strength and elongation,
 295 cracked and uncracked moduli, transition point location and energy dissipation
 296 capability is illustrated. It is found that temperature exposure may increase
 297 strength at the expense of ductility, and this outcome parallels similar findings

298 obtained in the context of pull-out [8] and tensile [25] tests. DSC analysis
299 reveals that temperature exposure may trigger competing processes: on the
300 one side further cross-linking is favoured in a post-curing process, on the other
301 side thermal degradation occurs. The final outcome strongly depends on the
302 considered epoxy coating and its post-curing capability. Indeed, in contrast to
303 the findings reported in [9], mild degradation is documented, especially when
304 compared to FRP systems. Temperature induces a monotonic decay in the
305 energy dissipation capability and, remarkably, the decay law, that is the same for
306 both coatings, complies with a cumulative Weibull distribution (power-law rule).
307 This behaviour is typical of models accounting for the relaxing and breaking of
308 molecular bonds in resins, as in [17, 11]. Therefore, this observation supports
309 the understanding that the resin degradation mechanism at the fabric-to-matrix
310 interface governs mechanical performance for both coatings.

311 **7. Acknowledgements**

312 The contribution of Dr. Jessica Morandi in specimen preparation is grate-
313 fully acknowledged.

314 **Funding**

315 AN gratefully acknowledges funding from "FAR Dipartimentali 2016", decr.
316 73/2017, prot. 37510.

317 **Declaration of interest**

318 Declarations of interest: none.

319 **Bibliography**

320 [1] D Arboleda. *Fabric Reinforced Cementitious Matrix (FRCM) Compos-*
321 *ites for Infrastructure Strengthening and Rehabilitation: Characterization*
322 *Methods*. PhD thesis, University of Miami, 2014. Open Access Dissertation.
323 Paper 1282.

- 324 [2] A Badanoiu and J Holmgren. Cementitious composites reinforced with
325 continuous carbon fibres for strengthening of concrete structures. *Cement*
326 *Concrete Comp*, 25(3):387–394, 2003.
- 327 [3] L Bisby, T Stratford, C Hart, and S Farren. Fire performance of well-
328 anchored TRM, FRCM and FRP flexural strengthening systems. In *Adv*
329 *Compos Constr*, Queen’s University Belfast, Sept. 2013.
- 330 [4] S Cao, WU Zhis, and X Wang. Tensile properties of CFRP and hybrid
331 FRP composites at elevated temperatures. *J Compos Mater*, 43(4):315–
332 330, 2009.
- 333 [5] A Çavdar. A study on the effects of high temperature on mechanical prop-
334 erties of fiber reinforced cementitious composites. *Compos Part B-Eng*, 43
335 (5):2452–2463, 2012.
- 336 [6] EU Chowdhury, R Eedson, LA Bisby, MF Green, and N Benichou. Mechan-
337 ical characterization of fibre reinforced polymers materials at high temper-
338 ature. *Fire Technol*, 47(4):1063–1080, 2011.
- 339 [7] CNR DT200. *Guide for the design and construction of an externally bonded*
340 *FRP system for strengthening existing structures*. Italian National Research
341 Council, Rome, 2004.
- 342 [8] SF de Andrade, M Butler, S Hempel, RD Toledo Filho, and V Mechtcher-
343 ine. Effects of elevated temperatures on the interface properties of carbon
344 textile-reinforced concrete. *Cement Concrete Comp*, 48:26–34, 2014.
- 345 [9] J Donnini, F De Caso y Basalo, V Corinaldesi, G Lancioni, and A Nanni.
346 Fabric-reinforced cementitious matrix behavior at high-temperature: Ex-
347 perimental and numerical results. *Compos Part B-Eng*, 108:108–121, 2017.
- 348 [10] SK Foster and LA Bisby. High temperature residual properties of exter-
349 nally bonded FRP systems. *Proceedings of the 7th international symposium*
350 *on fiber reinforced polymer reinforcement for reinforced concrete structures*
351 *(FRPRCS-7)*, SP-230-70, pages 1235–1252, 2005.

- 352 [11] AG Gibson, Y-S Wu, JT Evans, and AP Mouritz. Laminate theory analysis
353 of composites under load in fire. *J Compos Mater*, 40(7):639–658, 2006.
- 354 [12] CA Harper and EM Petrie. *Plastics materials and processes: a concise*
355 *encyclopedia*. John Wiley & Sons, 2003.
- 356 [13] O Homoro, M Michel, and TN Baranger. Pull-out response of glass yarn
357 from ettringite matrix: Effect of pre-impregnation and embedded length.
358 *Compos Sci Technol*, 170:174–182, 2018.
- 359 [14] ICC-Evaluation Service. Acceptance criteria for masonry and concrete
360 strengthening using fiber-reinforced cementitious matrix (FRCM) compos-
361 ite systems (AC434). *Whittier, CA*, 2013.
- 362 [15] M Jarrah, EP Najafabadi, MH Khaneghahi, and AV Oskouei. The effect
363 of elevated temperatures on the tensile performance of GFRP and CFRP
364 sheets. *Constr Build Mater*, 190:38–52, 2018.
- 365 [16] Y Li, X Liu, and M Wu. Mechanical properties of FRP-strengthened con-
366 crete at elevated temperature. *Constr Build Mater*, 134:424–432, 2017.
- 367 [17] CA Mahieux, KL Reifsnider, and SW Case. Property modeling across
368 transition temperatures in PMC’s: Part I. tensile properties. *Appl Compos*
369 *Mater*, 8(4):217–234, 2001.
- 370 [18] SR Maroudas and CG Papanicolaou. Effect of high temperatures on the
371 TRM-to-masonry bond. In *Key Engineering Materials*, volume 747, pages
372 533–541. Trans Tech Publ, 2017.
- 373 [19] M Messori, A Nobili, C Signorini, and A Sola. Mechanical performance
374 of epoxy coated AR-glass fabric Textile Reinforced Mortar: Influence of
375 coating thickness and formulation. *Compos Part B-Eng*, 149:135–143, 2018.
- 376 [20] A Nobili. Durability assessment of impregnated glass fabric reinforced ce-
377 mentitious matrix (GFRCM) composites in the alkaline and saline environ-
378 ments. *Constr Build Mater*, 105:465–471, 2016.

- 379 [21] A Nobili and FO Falope. Impregnated carbon fabric-reinforced cementi-
380 tious matrix composite for rehabilitation of the Finale Emilia hospital roofs:
381 case study. *J Compos Constr*, 21(4):05017001, 2017.
- 382 [22] A Nobili and C Signorini. On the effect of curing time and environmen-
383 tal exposure on impregnated carbon fabric reinforced cementitious matrix
384 (CFRCM) composite with design considerations. *Compos Part B-Eng*, 112:
385 300–313, 2017.
- 386 [23] L Ombres. Analysis of the bond between fabric reinforced cementitious
387 mortar (FRCM) strengthening systems and concrete. *Compos Part B-Eng*,
388 69:418–426, 2015.
- 389 [24] L Ombres. Structural performances of thermally conditioned PBO FRCM
390 confined concrete cylinders. *Compos Struct*, 176:1096–1106, 2017.
- 391 [25] DAS Rambo, F de Andrade Silva, RD Toledo Filho, and OFM Gomes.
392 Effect of elevated temperatures on the mechanical behavior of basalt textile
393 reinforced refractory concrete. *Mater Design*, 65:24–33, 2015.
- 394 [26] SM Raof and DA Bournas. TRM versus FRP in flexural strengthening
395 of RC beams: Behaviour at high temperatures. *Constr Build Mater*, 154:
396 424–437, 2017.
- 397 [27] RILEM Technical Committee 232-TDT. Test methods and design of textile
398 reinforced concrete. *Mater Struct*, 49(12):4923–4927, 2016. ISSN 1871-6873.
- 399 [28] M Saafi. Effect of fire on FRP reinforced concrete members. *Compos Struct*,
400 58(1):11–20, 2002. doi: 10.1016/S0263-8223(02)00045-4.
- 401 [29] C Scheffler, SL Gao, R Plonka, E Mäder, S Hempel, M Butler, and
402 V Mechtcherine. Interphase modification of alkali-resistant glass fibres and
403 carbon fibres for Textile Reinforced Concrete II: Water adsorption and
404 composite interphases. *Compos Sci Technol*, 69(7-8):905–912, 2009.

- 405 [30] C Signorini, A Nobili, and FO Falope. Mechanical performance and crack
406 pattern analysis of aged carbon fabric cementitious matrix (CFRCM) com-
407 posites. *Compos Struct*, 202:1114 – 1120, 2018. Special issue dedicated to
408 Ian Marshall.
- 409 [31] C Signorini, A Sola, A Nobili, and C Siligardi. Lime-cement Textile Rein-
410 forced Mortar (TRM) with modified interphase. *J Appl Biomater Funct*,
411 17(1):2280800019827823, 2019.
- 412 [32] Zoi C Tetta and Dionysios A Bournas. TRM vs FRP jacketing in shear
413 strengthening of concrete members subjected to high temperatures. *Com-
414 pos Part B-Eng*, 106:190–205, 2016.
- 415 [33] T Trapko. The effect of high temperature on the performance of CFRP
416 and FRCM confined concrete elements. *Compos Part B-Eng*, 54:138–145,
417 2013.
- 418 [34] S Xu, L Shen, J Wang, and Y Fu. High temperature mechanical perfor-
419 mance and micro interfacial adhesive failure of textile reinforced concrete
420 thin-plate. *J Zhejiang Univ-Sc A*, 15(1):31–38, 2014.